HHS Public Access

Author manuscript

Nat Struct Mol Biol. Author manuscript; available in PMC 2010 February 01.

Published in final edited form as:

Nat Struct Mol Biol. 2009 August ; 16(8): 833–839. doi:10.1038/nsmb.1642.

Structural and functional studies of the Ras-associating and pleckstrin-homology domains of Grb10 and Grb14

Rafael S Depetris[§,¶], **Jinhua Wu**[§], and **Stevan R Hubbard**[*]

Structural Biology Program, Kimmel Center for Biology and Medicine of the Skirball Institute, and Department of Pharmacology, New York University School of Medicine, New York, NY 10016

Abstract

Grb7, Grb10 and Grb14 are adapter proteins containing a Ras-associating (RA) domain, a pleckstrin-homology (PH) domain, a family-specific BPS (*b*etween *P*H and *S*H2) region, and a C-terminal Src-homology-2 domain. Previous structural studies showed that the Grb14 BPS region binds as a pseudosubstrate inhibitor in the tyrosine kinase domain of the insulin receptor to suppress insulin signaling. Here, we report the crystal structure of the RA and PH domains of Grb10 at 2.6 Å resolution. The structure reveals that these two domains, along with the intervening linker, form an integrated, dimeric structural unit. Biochemical studies demonstrated that Grb14 binds to activated Ras, which may serve as a timing mechanism for downregulation of insulin signaling. Our results illuminate not only membrane-recruitment mechanisms in Grb7-10-14, but also in MIG-10, Rap1-interacting adapter molecule, lamellipodin and Pico, proteins involved in actin-cytoskeleton rearrangement which share a structurally related RA-PH tandem unit.

INTRODUCTION

Grb7, Grb10 and Grb14 are related adapter proteins comprising an N-terminal region containing polyproline stretches, a Ras-associating (RA) domain, a pleckstrin-homology (PH) domain, a family-specific BPS (*b*etween *P*H and *S*H2) region and a C-terminal Src-homology-2 (SH2) domain1,2 (Fig. 1a). Using various biochemical approaches, these adapter proteins have been shown capable of binding to a variety of receptor tyrosine kinases, including the insulin and insulin-like growth factor-1 (IGF1) receptors1,2. Important insights into the true biological roles of Grb10 and Grb14 have come from gene-

[*]Correspondence: Dr. Stevan R. Hubbard, Skirball Institute of Biomolecular Medicine, New York University School of Medicine, 540 First Avenue, New York, NY 10016, phone: (212) 263-8938, fax: (212) 263-8951, e-mail: stevan.hubbard@med.nyu.edu.

[§]These authors contributed equally

[¶]Current address: Department of Microbiology and Immunology, Weill Medical College of Cornell University, 1300 York Ave. W-801, New York, NY 10065

AUTHOR CONTRIBUTIONS

R.S.D., crystallographic studies, in-cell biochemical experiments and manuscript preparation; J.W., structure refinement, fluorescence-polarization assays, in-cell biochemical experiments and manuscript preparation; S.R.H., project supervisor and principal manuscript author.

Accession codes

Atomic coordinates and structure factors for Grb10 RA-PH have been deposited in the Protein Data Bank with ID code 3HK0.

deletion studies in mice. The *Grb10* gene is maternally imprinted in mice, and loss of the maternal allele results in mice that are approximately 30% greater in size than wild-type littermates, with disproportionately large livers3. As adults, these mice exhibit improved glucose tolerance, increased muscle mass and reduced adiposity4,5. Transgenic mice overexpressing Grb10 show postnatal growth retardation and insulin resistance as a consequence of hyper-negative regulation of the insulin and IGF1 receptors6. Male *Grb14*$^{-/-}$ mice are of normal size and exhibit improved glucose tolerance and enhanced insulin signaling in muscle and liver7. These *in vivo* studies established that Grb10 and Grb14 are important tissue-specific negative regulators of insulin and IGF1 signaling.

Accumulating evidence suggests that Grb10 and Grb14 might contribute to type 2 (non-insulin-dependent) diabetes in humans. In the *ob/ob* mouse model for type 2 diabetes, Grb14 mRNA levels were increased by 75–100% in adipose tissue, and in type 2 diabetic patients, Grb14 mRNA levels were elevated by 43% in subcutaneous adipose tissue compared with non-diabetic control patients8. In a genome-wide association scan of an Amish population, the strongest association between type 2 diabetes and a single-nucleotide polymorphism was in the *Grb10* gene9.

We previously showed that the BPS region of Grb14 binds as a pseudosubstrate in the active site of the insulin receptor kinase to suppress substrate phosphorylation and thus downregulate insulin signaling10. The Grb14 SH2 domain binds to the phosphorylated activation loop of the kinase to increase the affinity and specificity of the Grb14-insulin receptor interaction10. In an effort to understand the roles of the RA and PH domains of Grb10 and Grb14 in inhibition of insulin signaling, we determined the crystal structure of the tandem RA and PH domains of human Grb10. The structure reveals that these two domains, along with the ~40-residue intervening linker, form an integrated RA-PH structural unit, which is dimerized via a helical extension of the PH domain. We provide evidence that Grb14 is a more potent inhibitor of insulin signaling than Grb10, and that both phosphoinositide and GTPase binding are crucial for downregulation of insulin signaling by Grb14. Our structural and biochemical data yield insights into the mechanisms of membrane recruitment not only for Grb7-10-14, but also for the so-called MRL proteins11: *M*IG-10[12], *R*ap1-interacting adapter molecule (RIAM)13,14, *l*amellipodin15 and Pico16, which are Ena/VASP-binding adapter proteins predicted to possess a similar RA-PH structural unit.

RESULTS

Crystal structure of Grb10 RA-PH

We engineered an *E. coli* expression construct to encode residues 106-357 of human Grb10, comprising the RA and PH domains, with a 6xHis-tag included on the N-terminus. Initial size-exclusion chromatography experiments on purified protein indicated that adventitious disulfide-bond formation was occurring (ten cysteines in this construct), leading to dimerization and higher-order oligomerization, despite the presence of reducing agent. To suppress disulfide-bond formation, we introduced four cysteine to serine substitutions (see Online Methods), based on their solvent exposure in available structures of RA and PH domain, at which point the protein ran as a single monomeric species on a size-exclusion column. This protein was nevertheless refractory to crystallization, and we introduced two

additional substitutions at presumed surface residues of the PH domain (K270A, E271A) to facilitate lattice interactions17. These substitutions did not affect phosphoinositide binding *in vitro* (data not shown). Crystals of this protein were obtained in monoclinic space group C2 with two Grb10 RA-PH molecules in the asymmetric unit (Ala270 and Ala271 are, in fact, in lattice contacts). The structure was determined by single anomalous diffraction (SAD) phasing of selenomethionyl-substituted protein crystals, and the structure was refined at 2.6 Å resolution. Data collection and refinement statistics are given in Table 1. Although disulfide-bond formation was apparently not an obstacle to crystallization of Grb14 RA-PH (only four cysteines, no evidence of disulfide formation), we were unable to obtain crystals of wild-type Grb14 RA-PH or the double mutant K272A/E273A.

The crystal structure of Grb10 RA-PH reveals canonically folded RA and PH domains with two exceptional features: an extensive interface between the two domains and the intervening linker, and a dimerized RA-PH unit via a C-terminal helical extension of the PH domain (Fig. 1b). The RA domain adopts the ubiquitin-like fold observed for other RA domains such as those from c-Raf18 and RalGDS19, comprising a five-stranded β sheet and three short α helices. The Grb10 PH domain comprises a seven-stranded (anti-parallel) β sandwich and a C-terminal α helix. In contrast to canonical PH domains, which terminate after the C-terminal helix, the polypeptide chain in the Grb10 PH domain undergoes an approximately 90° turn after this helix, facilitated by conserved Gly342, and then forms a two-turn α helix (α2 in Fig. 1b). This helical extension to the Grb10 PH domain is involved in dimerization of RA-PH (Fig. 1c, detailed below).

The RA and PH domains are adjoined through an anti-parallel β-strand interaction: β4 of the RA domain with β5 of the PH domain. The RA-PH interface buries a total surface area of 1,326 $Å^2$ and is fortified by a number of van der Waals and hydrogen-bonding interactions. Two hydrophobic residues from each domain—Leu160 and Leu162 (RA) and Phe287 and Leu318 (PH)—interdigitate to form a small hydrophobic cluster in the interface (Fig. 1d and Supplementary Fig. 1 online (electron density map)). The hydrophobicity of these residues is conserved in Grb7-10-14 (Fig. 2a) and in the MRL proteins (Supplementary Fig. 2 online). In “stand-alone” RA and PH domains, the corresponding residues are typically hydrophilic. A salt bridge is made between Glu167 (RA) and Arg337 (PH), both of which are conserved in Grb7-10-14 and in the MRL proteins, and several hydrogen-bonding interactions are present in the interface. Limited trypsin digestion of Grb10 and Grb14 RA-PH, which separates the two domains, followed by size-exclusion chromatography confirmed the physical association of the domains (data not shown). In this configuration of the RA and PH domains, both the Ras (or other small GTPase) binding site in the RA domain and the phosphoinositide binding site in the PH domain are accessible (Fig. 1b, note positions of labels ‘RA’ and ‘PH’).

The linker between the RA and PH domains of Grb10 comprises approximately 40 residues that are well conserved in Grb7-10-14 (Fig. 2a), but less conserved in the MRL proteins (Supplementary Fig. 2 online). In the Grb10 RA-PH structure, residues in the linker form two short α helices and one β strand, the latter of which augments (in an anti-parallel fashion) β1 of the PH domain. The linker interacts primarily with the PH domain and its C-terminal helical extension (α2) via Grb7-10-14-conserved (hydrophobicity) Tyr194, Phe196,

Phe197, Phe203, Phe204, Met208, Val209, Leu223, Leu224, Phe227 and Leu228 (Supplementary Fig. 3 online). These contacts appear to stabilize the position of α2 for dimerization.

In the crystal structure, the two RA-PH molecules in the asymmetric unit are related by an approximate two-fold axis (174° rotation, 0.5 Å translation). The dimerization interface buries a total surface area of 1,566 $Å^2$, and the contributing residues are mainly from the C-terminal helical extension (α2) of the PH domain (Met343, Leu344, Tyr346, Gln347, Asn348 and Arg350) and also from the RA-PH linker (Gln224 and Asn228) (Fig. 1c). These residues are relatively well conserved in Grb7-10-14 (Fig. 2a). At high loading concentrations (>20 mg/ml), a dimer peak as well as a monomer peak is evident by size-exclusion chromatography, suggesting that the K_d for dimerization in solution is relatively high (see Discussion). A double-alanine substitution (Q347A/N348A) in the dimer interface suppresses dimer formation (Supplementary Fig. 4 online).

Phosphoinositide binding to Grb10 and Grb14

Because a majority of PH domains bind to membrane phosphoinositides, we characterized the phosphoinositide binding specificities of Grb10 and Grb14 RA-PH using BODIPY TMR-conjugated phosphoinositides in a fluorescence-polarization assay20. Grb10 RA-PH bound to several phosphoinositides—PI(5)P, PI(4,5)P_2, PI(3,4)P_2, and PI(3,4,5)P_3—with affinities (K_d values) in the 4 to 10 μM range, and bound poorly to all others (Fig. 3a and Table 2). These data indicate that the Grb10 PH domain binds relatively non-specifically to phosphoinositides and with modest affinities, characteristics that are common among PH domains21. Using the same fluorescence-polarization assay, we also measured the phosphoinositide binding constants for Grb14 RA-PH (Fig. 3b and Table 2). Despite 64% sequence identity in the PH domains of Grb10 and Grb14, the Grb14 PH domain bound to phosphoinositides with lower affinity. The best binder was PI(3,4,5)P_3 with a K_d of 28 μM. All other phosphoinositides bound weakly with K_d values > 90 μM.

Most phosphoinositide-binding PH domains engage the headgroup “atop” the loop connecting the β1 and β2 strands (Fig. 3c). A subset of PH domains, including β-spectrin22, Tiam1 and ArhGAP920, bind headgroups via a non-canonical mode, in which the headgroup binds on the “side” of β2 and interacts with the β5-β6 loop as well (Fig. 3d). A sequence alignment of Grb10 and Grb14 with various PH domains (Fig. 2b) suggests that phosphoinositides may bind non-canonically to the Grb10 and Grb14 PH domains. Canonical-binding PH domains (e.g., Grp123,24 and Akt25) contain a lysine or arginine two residues C-terminal to a buried hydrophobic residue in β1 (Leu239 in Grb10) (Fig. 2b). In Grb10, Grb14 and ArhGAP9, a hydrophobic residue is positioned here (Val241 in Grb10). Non-canonical-binding PH domains usually contain instead a basic residue three residues C-terminal to the conserved hydrophobic residue, as do Grb10 (Lys242) and Grb14 (Lys244). Strikingly, the next residue in Grb10 and Grb14 is a glutamic acid (Glu243/245 in Grb10/14), which would be predicted to hinder headgroup binding at the canonical site, both sterically and electrostatically (Fig. 3c). β-spectrin and ArhGAP9 also contain residues with large (although not acidic) side chains at this position. Interestingly, in Grb7, this residue is a glycine, as in Grp1 and Akt, which bind PI(3,4,5)P_3 canonically.

In the β5-β6 loop, less sequence similarity is exhibited between β-spectrin, ArhGAP9, and Grb7-10-14 (Fig. 2b), and therefore it is more difficult to predict which residues in the β5-β6 loop of Grb7-10-14 might be involved in binding headgroups non-canonically. Although there are several basic residues in this loop in Grb7-10-14, their positioning in the Grb10 RA-PH structure indicates that they are unlikely to interact directly with phosphate groups of the headgroup. One residue in the β5-β6 loop of Grb10 that appears to be positioned for headgroup binding is Asn297, which is a glycine in Grb14.

Unfortunately, attempts to co-crystallize (or soak) Grb10 RA-PH with various phosphoinositide headgroups were unsuccessful. To explore the phosphoinositide binding modes utilized by Grb10 and Grb14, we introduced several individual point mutations into Grb10 and Grb14 RA-PH and measured phosphoinositide binding using the fluorescence-polarization assay. The results are presented in Table 2. Three lysine-to-alanine mutations were made in the β1-β2 loop of Grb10: K242A, K247A and K250A. Lys242 and Lys247 are positioned to interact with headgroups only in the non-canonical binding mode (Fig. 3d), and these mutations resulted in approximately a two- and five-fold loss of binding, respectively (Table 2). Lys250 could interact with the 1-phosphate group in either binding mode (canonical or non-canonical), and mutation to alanine also resulted in a five-fold loss of binding.

The case for non-canonical binding is strengthened by the N297G mutation in the β5-β6 loop of the Grb10 PH domain, which also resulted in a five-fold loss of binding (Table 2), and the E243G/L244S mutation in the β1-β2 loop, which had no appreciable effect on headgroup binding, but would be predicted to increase canonical binding in the absence of an alternative binding mode (Fig. 3c). In Grb14, this same mutation resulted in a four-fold increase in PI(3,4,5)P_3 binding, while replacement of Gly299 with asparagine (β5-β6 loop) did not result in higher (Grb10-like) binding affinities. The mutation K252A in Grb14 (K250A in Grb10) decreased PI(3,4,5) binding affinity by more than three-fold (Table 2).

Ras binding to Grb10 and Grb14

Previous pulldown experiments using cell lysates demonstrated that Grb7 (Grb10/14 not tested) binds to activated Ras (N-, K-, and H-Ras) and much weaker to activated Rap1 and Rap226. In a similar fashion, we co-transfected HEK 293T cells with HA-tagged, wild-type N-Ras or a constitutively active mutant (G12D), along with Myc-tagged Grb7, Grb10 or Grb14 (all full-length), immunoprec [0-9]^13 ipitated N-Ras with an anti-HA antibody and immunoblotted for Grb7-10-14 using an anti-Myc antibody. This co-immunoprecipitation experiment (Fig. 4a) demonstrated that Grb14, like Grb7, interacts with N-Ras, but that Grb10 interacts comparatively weakly. This experiment also showed that Grb7-10-14 bind preferentially to activated N-Ras. Pulldown experiments using lysates of HEK 293T cells co-transfected with either constitutively active N-Ras, Rap1 or Rap2 (GST fusions) and Grb10 or Grb14 demonstrated that Grb10 and Grb14 do not bind appreciably to Rap1 or Rap2 relative to N-Ras (data not shown).

A point mutation in the Grb14 RA domain, K140A (Lys142 in Grb10), was introduced to verify that the mode of binding of the Grb14 RA domain to activated Ras is similar to that of other RA domain-GTPase interactions, for example, RalGDS(RA) with Ras27. Indeed, this

mutation disrupted the interaction between Grb14 and N-Ras as evidenced by the loss of co-immunoprecipitation (Fig. 4b).

To determine whether the PH domain is important for the interaction of Grb14 with Ras, we tested the binding of Grb14 K252A to Ras. This mutation in Grb14 RA-PH resulted in loss of binding of phosphoinositide headgroups *in vitro* (Table 2). The reduced co-immunoprecipitation with Ras for this PH-domain mutation (Fig. 4b) indicates that Grb14 membrane association, mediated by the PH domain, is important for the interaction of Grb14 with Ras.

Grb14 RA-PH is required for inhibition of insulin signaling

To probe the contributions of the RA and PH domains to inhibition of insulin signaling by Grb10 and Grb14, we transiently transfected wild-type Grb10 or Grb14, or selected point mutants, into Chinese hamster ovary cells stably transfected with the insulin receptor (CHO-IR) and monitored phosphorylation of Akt and extracellular signal-related kinase (ERK). These two serine/threonine kinases are activated through the phosphatidylinositol 3-kinase (PI-3K) and Ras pathways, respectively, subsequent to phosphorylation of insulin receptor substrate (IRS) proteins. Compared to the non-transfected control, introduction of wild-type Grb14 into CHO-IR cells dramatically diminished insulin-stimulated Akt phosphorylation (Fig. 5a). Both the RA-(K140A) and PH-domain (K252A) mutations compromised the ability of Grb14 to inhibit Akt activation. Mutation of the dimerization interface in the C-terminal helical extension to the PH domain also resulted in loss of inhibition (QNAA in Fig. 5a). Compared to Grb14, Grb10 was a much less potent inhibitor of Akt activation. For inhibition of ERK phosphorylation, the results are similar, if somewhat less striking (Fig. 5a). Again, Grb14 was a more potent inhibitor of ERK phosphorylation than Grb10, and point mutations in the Grb14 RA domain (K140A), PH domain (K252A) or the RA-PH dimerization interface (QNAA) compromised the inhibitory effect of Grb14. Grb10 was also a poor inhibitor of insulin-stimulated ERK phosphorylation.

Presumably, the inability of Grb14 to attenuate insulin signaling upon mutation of the RA or PH domain is due to less efficient recruitment of Grb14 to the insulin receptor. To test this, we performed co-immunoprecipitation experiments in CHO-IR cells transfected with wild-type or mutant Grb14. The Grb14 point mutations K140A (RA domain) and K252A (PH domain) resulted in a partial loss of interaction between Grb14 and the insulin receptor (Fig. 5b), although there was no appreciable difference in receptor association for the RA-PH dimerization mutant (QNAA). Compared to Grb14, Grb10 interacts poorly with the insulin receptor (Fig. 5b), consistent with its weaker ability to inhibit insulin signaling (Fig. 5a). Because the co-immunoprecipitation experiment is performed with detergent-solubilized membranes, we also performed fluorescence microscopy studies on intact CHO-IR cells transfected with GFP-Grb14, which showed that GFP-Grb14 K252A remains in the cytoplasm upon insulin stimulation, in contrast to wild-type GFP-Grb14, which translocates to the plasma membrane (Supplementary Fig. 5 online).

DISCUSSION

After insulin stimulation, the insulin receptor is downregulated by several mechanisms, including dephosphorylation by protein tyrosine phosphatases such as PTP1B28,29 and binding of the adapter protein Grb147. The BPS region in Grb14 directly inhibits the catalytic activity of the insulin receptor by binding as a pseudosubstrate in the kinase active site, and the C-terminal SH2 domain binds to the phosphorylated activation loop10. Our current structural and biochemical studies focused on the RA and PH domains of Grb10 and Grb14, and demonstrated that they, in addition to the BPS region and SH2 domain, are required for inhibition of insulin signaling by Grb14 (Fig. 5a).

The crystal structure of Grb10 RA-PH reveals that these two domains, separated in sequence by ~40 residues, nevertheless physically associate to form a single structural unit. The RA-PH interface is conserved in Grb14 and Grb7. We propose that the role of the integrated RA-PH structural unit is to optimize binding of small GTPases (*e.g.*, Ras) at the plasma membrane. That is, binding of the PH domain to membrane phosphoinositides will favorably position the structurally coupled RA domain for binding to membrane-anchored GTPases. As judged from the Grb14-Ras-insulin receptor structural model (Fig. 6), the particular mechanism of membrane anchoring of a GTPase—N-terminal (*e.g.*, Arf proteins) versus C-terminal (*e.g.*, Ras proteins), length of the tether—could dictate whether a given GTPase will interact with an RA-PH unit, in addition to the intrinsic GTPase-RA domain binding affinity. For example, the Rap1 C-terminal tail is seven residues shorter than that of N-Ras, which could explain, in part, why Rap1 binds poorly to Grb14 (data not shown) and Grb726.

Most PH domains bind to membrane phosphoinositides and do so with modest affinities21. The measured binding affinities to the Grb10 PH domain are in the 4–10 μM K_d range (for PIP_2 and PIP_3, Table 2), whereas for the Grb14 PH domain, the range is ≥30 μM. The sequences of the Grb10 and Grb14 PH domains, particularly a glutamic acid in the β1-β2 loop (Glu243 in Grb10) (Fig. 3c), suggested that these PH domains may bind phosphoinositides non-canonically20. The mutagenesis data (Table 2), although not unequivocal, indicate that the Grb10 PH domain binds phosphoinositides non-canonically, but that the Grb14 PH domain may bind phosphoinositides canonically. Because Grb14 RA-PH showed modest *in vitro* specificity toward $PI(3,4,5)P_3$ (Fig. 3b), we tested whether wortmannin, an inhibitor of PI-3K, affects the ability of Grb14 to be recruited to the insulin receptor. The co-immunoprecipitation results (data not shown) suggest that PI-3K activity is not required for Grb14 recruitment to the receptor.

Interestingly, PH domains have been implicated in binding directly to activated GTPases30, raising the question whether the Grb14 PH domain, which binds phosphoinositides weakly, could bind directly to GTPases together with the RA domain. Based on the relative position of the RA and PH domains in the Grb10 RA-PH structure and the mode of GTPase binding to an RA domain18,27 (with corroboration from the Grb14 K140A result (Fig. 4b)), a direct interaction between the Grb14 PH domain and a GTPase appears unlikely.

Grb14 binds better to activated Ras than Grb10 (Fig. 4a), although it is not clear from the Grb10 RA-PH structure and a sequence comparison of the RA domains why this might be so. Because membrane recruitment via the PH domain is important for the interaction of Grb14 with Ras (K252A in Fig. 4b), differences in the phosphoinositide binding characteristics of the PH domains of Grb10 and Grb14 might account for the differential ability to interact with Ras. It is conceivable that the higher-affinity (and more promiscuous) PH domain of Grb10 results in recruitment to different regions of the plasma membrane than Grb14, or perhaps to internal membranes. Of note, dimerization of the RA-PH unit through the C-terminal extension of the PH domain will increase membrane binding avidity21. Although Grb10 RA-PH only weakly dimerizes in solution (Supplementary Fig. 4 online), dimerization of the Grb10/14 SH2 domain31, along with membrane association of the PH domain, will enhance formation of the RA-PH dimer.

Our functional studies monitoring Akt and ERK activation downstream of insulin stimulation demonstrated that Grb14 is a more potent inhibitor of insulin signaling than Grb10 (Fig. 5a), at least in CHO-IR cells, which is probably due to more efficient recruitment of Grb14 to the insulin receptor (Fig. 5b). Previous biochemical experiments showed that the Grb14 BPS region is a more potent inhibitor (and thus better binder) of the insulin receptor than the Grb10 BPS region32. Our data demonstrating that Grb10 is a weak binder of Ras compared to Grb14 (Fig. 4a), and that GTPase is evidently necessary for full recruitment of Grb14 to the insulin receptor (K140A in Fig. 5b), indicate that the RA-PH unit of Grb14 also contributes to its inhibitory signaling potency versus Grb10. In light of these biochemical results for Grb10, it is somewhat surprising that *Grb10*$^{-/-}$ mice display an improved insulin-signaling phenotype4,5, although the expression levels of Grb10 versus Grb14 in insulin-responsive cells has not been characterized.

The tandem RA-PH domains of Grb7-10-14 are conserved in a second adapter-protein family (MRL proteins11) comprising the *Caenorhabditis elegans* protein MIG-10[12], the mammalian proteins RIAM13,14 and lamellipodin12 and the *Drosophila melanogaster* protein Pico12, all of which are Ena/VASP-binding proteins involved in actin-cytoskeleton rearrangement. Genetic evidence indicates that MIG-10 interacts with the small GTPase CED-10/Rac133. RIAM, although named for its ability to interact with Rap113, was shown in a different study to bind instead to Ras14. Despite efforts to do so, no small GTPase has been identified as a lamellipodin binder15. The PH domains of RIAM and lamellipodin, like Grb10 and Grb14, contain an acidic residue in the β1-β2 loop (Glu243 in Grb10, Supplementary Fig. 2 online), which suggests that these PH domains might bind phosphoinositides via the non-canonical mode. Whether in RA-PH-containing proteins the phosphoinositide binding mode influences GTPase binding or specificity remains to be determined.

In response to insulin, a number of cellular signaling pathways are activated, including the PI-3K and ERK pathways, which are then attenuated at the level of the insulin receptor by PTP1B and Grb14. The mechanisms that govern the kinetics of insulin signaling are not well understood, in particular, how the duration of positive signaling is controlled. Dephosphorylation of the insulin receptor by endoplasmic reticulum-tethered PTP1B is thought to require endocytosis of the receptor, and the time scale for this process (minutes)

provides a window of opportunity for recruitment and phosphorylation of IRS proteins to activate the PI-3K and ERK pathways. In contrast, the negative regulator Grb14 is a multi-domain cytoplasmic adapter protein, not unlike the PH-PTB-containing IRS proteins, which binds to the phosphorylated (activated) kinase domain of the insulin receptor. We have shown here that Grb14-mediated inhibition of insulin signaling requires functional RA and PH domains, and that Grb14 can bind to activated Ras. Therefore, an attractive hypothesis is that Ras activation serves as a timing mechanism for the negative-feedback inhibition of insulin signaling by Grb14.

METHODS

Protein expression and purification

We subcloned the cDNA encoding residues 106-357 (RA and PH domains) of human Grb10 (isoform c) into the expression vector pET14b (Novagen). We introduced the cysteine mutations C331S, C232S, C145S and C212S sequentially to abrogate disulfide-bond formation. In addition, we introduced two mutations to facilitate crystal-packing interactions: K270A and E271A. We grew cultures of BL21(DE3) in Luria broth media at 37 °C and induced with 1 mM IPTG at 30 °C. We harvested the cells and resuspended them in lysis buffer (50 mM Tris (pH 8.0), 300 mM NaCl, 0.1% (w/v) Triton X-100, and complete EDTA-free protease inhibitor cocktail (Roche Diagnostics)), lysed them by French press and clarified by centrifugation. We isolated the 6xHis-tagged protein by Ni^{2+}-affinity chromatography (Sigma), cleaved with thrombin to remove the tag, and further purified the protein by Superdex 75 and Source S chromatography (GE Healthcare). The purified protein included Grb10 residues 106-357 and four heterologous residues (GSHM) on the N-terminus remaining from the thrombin cleavage site. We performed site-directed mutagenesis on Grb10 RA-PH (and on all other constructs) using the QuikChange system (Stratagene), and verified all constructs by DNA sequencing.

To produce selenomethionyl-labeled Grb10 RA-PH, we transformed BL21(DE3) cells from 1 ml of an overnight culture in LB medium, spun down in 1 ml of M9 minimal medium with carbon source at 4 g l^{-1}, and then added to one liter of the same pre-warmed medium. Cells were grown to mid-log phase before addition of the following amino acids: lysine, phenylalanine and threonine at 100 mg l^{-1}; isoleucine, leucine and valine at 50 mg l^{-1}; and L-selenomethionine at 60 mg l^{-1}. We induced with 1 mM IPTG 15 min after addition of the amino acids.

For fluorescence-polarization measurements, we expressed the 6xHis-tagged Grp1 PH domain in *E. coli* strain BL21(DE3) and induced overnight with 0.1 mM IPTG at 20 °C. We purified the protein by Ni^{2+}-affinity chromatography (Sigma) followed by Superdex 75 chromatography, and concentrated the purified protein to 10 mg ml^{-1} for the phospholipid-binding studies.

X-ray crystallography

We concentrated Grb10 RA-PH to 25 mg ml^{-1} and grew native and selenomethionyl (SeMet)-derivatized crystals at 17 °C in hanging drops containing equal volumes of protein

solution and reservoir buffer (~15% (w/v) PEG 3350, 0.15 M sodium thiocyanate and 1 mM dithiothreitol (DTT)). Crystals of native and SeMet Grb10 RA-PH belong to space group C2 (see Table 1 for unit-cell constants). There are two Grb10 RA-PH molecules in the asymmetric unit (solvent content 41%). Before flash freezing in liquid nitrogen, we equilibrated crystals in a series of stabilizing solutions containing reservoir buffer plus 10%, 15%, 20% then 25% (v/v) ethylene glycol. We collected data from native and SeMet crystals on beam line X4A at the National Synchrotron Light Source, Brookhaven National Laboratory near the wavelength corresponding to the peak of absorption (K-edge) for selenium (0.9789 Å). We processed diffraction data using HKL200035 and determined the Grb10 RA-PH structure by SAD (single anomalous diffraction) phasing using SOLVE/RESOLVE36, based on the data obtained from a single SeMet-derivatized crystal (figure of merit=0.41 from SOLVE, 0.68 after RESOLVE; 30-2.9 Å). We found twelve ordered Se atoms in the two copies of Grb10 RA-PH in the asymmetric unit, representing 11 of the 12 possible sites (not including the disordered N-terminal SeMet (GSHM) remaining from thrombin cleavage). We performed model building with Coot37 and refinement (at 2.6 Å) with CNS38 and REFMAC39, using the native data set. The final atomic model contains residues 110-350, excluding 143-149 (in the RA domain) and 216-221 (in the RA-PH linker) (copy A), and residues 111-350, excluding 143-148, 213-221, and 265-273 (copy B).

Phosphoinositide binding measurements

We mixed purified Grb10 or Grb14 RA-PH at concentrations ranging from 0.8 μM to 100 μM, or buffer only, with 12.5 nM (final) of BODIPY TMR-labeled phosphoinositides (Echelon) in a buffer containing 20 mM HEPES (pH 7.5), 150 mM NaCl and 0.05% (v/v) Tween-20. After 5 min of incubation, we added 20 μl of the reaction mix to individual wells of a 384-well assay plate (Corning), then measured fluorescence polarization at room temperature using a TECAN Infinite F500 plate reader. We used a 535/25 nm filter as an excitation filter, and a pair of 590/20 nm filters as emission polarization filters. We subtracted the buffer-only data from the protein data, and performed curve fitting to a single-site (saturating) binding model using SigmaPlot (Systat Software).

Cell transfection, immunoprecipitation, and immunoblotting

We subcloned the cDNA for Grb7 (mouse), Grb10 (human, isoform c), and Grb14 (human) into a pRK5 vector containing an N-terminal Myc tag. We transfected CHO-IR cells using Lipofectamine 2000 reagent (Invitrogen) for 6 h. After 24 h, we serum-deprived the cells for 3 h in Ham's F-12 medium, treated the cells with 5 nM insulin for 5 min, washed twice in ice-cold phosphate-buffered saline and lysed for 20 min at room temperature with buffer containing 50mM Tris-HCl (pH 8.0), 100 mM NaCl, 1% (v/v) Triton X-100 and phosphatase- and protease-inhibitor cocktails (Roche Diagnostics). We clarified the lysates by centrifugation and added SDS-PAGE sample buffer. We resolved the proteins by SDS-PAGE and transferred them to Immobilon-P polyvinylidene difluoride membranes (Millipore). We detected individual proteins with the following antibodies: anti-insulin receptor β subunit (C-19, Santa Cruz Biotechnology); anti-insulin receptor pTyr1162/1163 (BioSource International); anti-ERK1/2, anti-pERK1/2 (Thr202/Tyr204), anti-Akt, anti-pAkt (pSer473) (Cell Signaling Technology); and anti-Myc (9E10) (Santa Cruz

Biotechnology). We visualized the bands by blotting with horseradish peroxidase-conjugated secondary antibodies (Santa Cruz Biotechnology).

For co-immunoprecipitation studies of the insulin receptor with Grb10/14, we transfected CHO-IR cells, stimulated with insulin and lysed the cells as described above. Subsequently, we clarified the lysate by centrifugation and incubated overnight with the anti-insulin receptor βsubunit antibody. We incubated with protein A/G PLUS-agarose beads (Santa Cruz Biotechnology) for 1 h at 4 °C, and then we centrifuged the beads and extensively washed them with lysis buffer (above) containing 0.1% Triton X-100 before solubilization in SDS-PAGE buffer. We resolved bound proteins by SDS-PAGE and immunoblotted using the anti-Myc antibody.

For co-immunoprecipitation studies of Grb7-10-14 with N-Ras, we used for the latter a pCGN vector containing an N-terminal HA tag. We co-transfected HEK 293T cells with Myc-tagged Grb7, -10 or -14 and HA-tagged N-Ras (wild-type or G12D) following the procedures described above. After 24 h, we lysed the cells with 20 mM Tris-HCl (pH 7.5), 150 mM NaCl, 5 mM $MgCl_2$, 1% Triton X-100, 1 mM DTT and phosphatase- and protease-inhibitor cocktails (Roche Diagnostics). We clarified the lysates by centrifugation and incubated overnight with anti-HA antibody (F-7) (Santa Cruz Biotechnology) at 4 °C. We subsequently incubated this mixture with protein A/G PLUS-agarose beads for 1 h at 4 °C, then centrifuged the beads and extensively washed them with lysis buffer (except 0.1% instead of 1% Triton X-100) before solubilizing with SDS-PAGE buffer. We resolved bound proteins by SDS-PAGE and immunoblotted using the anti-HA and anti-Myc (9E10) antibodies.

Supplementary Material

Refer to Web version on PubMed Central for supplementary material.

Acknowledgments

This work was supported by National Institutes of Health grant DK052916 (to S.R.H.) We thank Dr. Rodolfo Ghirlando for sedimentation velocity measurements, Dr. Mark Philips (NYU School of Medicine) for HA-tagged Ras vectors and discussions, Dr. Frank McCormick (University of California at San Francisco) for the GST-Ras/Rap vectors, Dr. David Lambright (University of Massachusetts Medical School) for the Grp1 PH domain construct, Dr. Derek Ceccarelli for assistance in the fluorescence-polarization experiments, Dr. Todd Miller for critical reading of the manuscript, and Nupur Hiremath and Julia Burrill for technical assistance. Beamline X4A at the National Synchrotron Light Source, Brookhaven National Laboratory, a DOE facility, is supported by the New York Structural Biology Consortium.

References

1. Han DC, Shen TL, Guan JL. The Grb7 family proteins: structure, interactions with other signaling molecules and potential cellular functions. Oncogene. 2001; 20:6315–21. [PubMed: 11607834]
2. Holt LJ, Siddle K. Grb10 and Grb14: enigmatic regulators of insulin action - and more? Biochem J. 2005; 388:393–406. [PubMed: 15901248]
3. Charalambous M, et al. Disruption of the imprinted Grb10 gene leads to disproportionate overgrowth by an Igf2-independent mechanism. Proc Natl Acad Sci USA. 2003; 100:8292–7. [PubMed: 12829789]

4. Smith FM, et al. Mice with a disruption of the imprinted Grb10 gene exhibit altered body composition, glucose homeostasis, and insulin signaling during postnatal life. Mol Cell Biol. 2007; 27:5871–86. [PubMed: 17562854]
5. Wang L, et al. Peripheral disruption of the Grb10 gene enhances insulin signaling and sensitivity in vivo. Mol Cell Biol. 2007; 27:6497–505. [PubMed: 17620412]
6. Shiura H, et al. Meg1/Grb10 overexpression causes postnatal growth retardation and insulin resistance via negative modulation of the IGF1R and IR cascades. Biochem Biophys Res Commun. 2005; 329:909–16. [PubMed: 15752742]
7. Cooney GJ, et al. Improved glucose homeostasis and enhanced insulin signalling in Grb14-deficient mice. EMBO J. 2004; 23:582–593. [PubMed: 14749734]
8. Cariou B, et al. Increased adipose tissue expression of Grb14 in several models of insulin resistance. FASEB J. 2004; 18:965–7. [PubMed: 15059968]
9. Rampersaud E, et al. Identification of novel candidate genes for type 2 diabetes from a genome-wide association scan in the Old Order Amish: evidence for replication from diabetes-related quantitative traits and from independent populations. Diabetes. 2007; 56:3053–62. [PubMed: 17846126]
10. Depetris RS, Hu J, Gimpelevich I, Holt LJ, Hubbard SR. Structural basis for inhibition of the insulin receptor by the adaptor protein Grb14. Mol Cell. 2005; 20:325–333. [PubMed: 16246733]
11. Holt LJ, Daly RJ. Adapter protein connections: the MRL and Grb7 protein families. Growth Factors. 2005; 23:193–201. [PubMed: 16243711]
12. Manser J, Roonprapunt C, Margolis B. C elegans cell migration gene mig-10 shares similarities with a family of SH2 domain proteins and acts cell nonautonomously in excretory canal development. Dev Biol. 1997; 184:150–164. [PubMed: 9142991]
13. Lafuente EM, et al. RIAM, an Ena/VASP and Profilin ligand, interacts with Rap1-GTP and mediates Rap1-induced adhesion. Dev Cell. 2004; 7:585–95. [PubMed: 15469846]
14. Jenzora A, Behrendt B, Small JV, Wehland J, Stradal TE. PREL1 provides a link from Ras signalling to the actin cytoskeleton via Ena/VASP proteins. FEBS Lett. 2005; 579:455–63. [PubMed: 15642358]
15. Krause M, et al. Lamellipodin, an Ena/VASP ligand, is implicated in the regulation of lamellipodial dynamics. Dev Cell. 2004; 7:571–83. [PubMed: 15469845]
16. Lyulcheva E, et al. Drosophila pico and its mammalian ortholog lamellipodin activate serum response factor and promote cell proliferation. Dev Cell. 2008; 15:680–90. [PubMed: 19000833]
17. Derewenda ZS. Rational protein crystallization by mutational surface engineering. Structure (Camb). 2004; 12:529–35. [PubMed: 15062076]
18. Nassar N, et al. The 2.2 A crystal structure of the Ras-binding domain of the serine/threonine kinase c-Raf1 in complex with Rap1A and a GTP analogue. Nature. 1995; 375:554–60. [PubMed: 7791872]
19. Huang L, Weng X, Hofer F, Martin GS, Kim SH. Three-dimensional structure of the Ras-interacting domain of RalGDS. Nat Struct Biol. 1997; 4:609–15. [PubMed: 9253406]
20. Ceccarelli DF, et al. Non-canonical interaction of phosphoinositides with pleckstrin homology domains of Tiam1 and ArhGAP9. J Biol Chem. 2007; 282:13864–74. [PubMed: 17339315]
21. Lemmon MA, Ferguson KM. Signal-dependent membrane targeting by pleckstrin homology (PH) domains. Biochem J. 2000; 350(Pt 1):1–18. [PubMed: 10926821]
22. Hyvonen M, et al. Structure of the binding site for inositol phosphates in a PH domain. EMBO J. 1995; 14:4676–85. [PubMed: 7588597]
23. Ferguson KM, et al. Structural basis for discrimination of 3-phosphoinositides by pleckstrin homology domains. Mol Cell. 2000; 6:373–84. [PubMed: 10983984]
24. Lietzke SE, et al. Structural basis of 3-phosphoinositide recognition by pleckstrin homology domains. Mol Cell. 2000; 6:385–94. [PubMed: 10983985]
25. Thomas CC, Deak M, Alessi DR, van Aalten DM. High-resolution structure of the pleckstrin homology domain of protein kinase b/akt bound to phosphatidylinositol (3,4,5)-trisphosphate. Curr Biol. 2002; 12:1256–62. [PubMed: 12176338]

26. Rodriguez-Viciana P, Sabatier C, McCormick F. Signaling specificity by Ras family GTPases is determined by the full spectrum of effectors they regulate. Mol Cell Biol. 2004; 24:4943–54. [PubMed: 15143186]
27. Huang L, Hofer F, Martin GS, Kim SH. Structural basis for the interaction of Ras with RalGDS. Nat Struct Biol. 1998; 5:422–6. [PubMed: 9628477]
28. Elchebly M, et al. Increased insulin sensitivity and obesity resistance in mice lacking the protein tyrosine phosphatase-1B gene. Science. 1999; 283:1544–1548. [PubMed: 10066179]
29. Klaman LD, et al. Increased energy expenditure, decreased adiposity, and tissue-specific insulin sensitivity in protein-tyrosine phosphatase 1B-deficient mice. Mol Cell Biol. 2000; 20:5479–5489. [PubMed: 10891488]
30. Lemmon MA. Pleckstrin homology domains: not just for phosphoinositides. Biochem Soc Trans. 2004; 32:707–11. [PubMed: 15493994]
31. Stein EG, Ghirlando R, Hubbard SR. Structural basis for dimerization of the Grb10 Src homology 2 domain. Implications for ligand specificity. J Biol Chem. 2003; 278:13257–64. [PubMed: 12551896]
32. Bereziat V, et al. Inhibition of insulin receptor catalytic activity by the molecular adapter Grb14. J Biol Chem. 2002; 277:4845–52. [PubMed: 11726652]
33. Quinn CC, Pfeil DS, Wadsworth WG. CED-10/Rac1 mediates axon guidance by regulating the asymmetric distribution of MIG-10/lamellipodin. Curr Biol. 2008; 18:808–13. [PubMed: 18499456]
34. Hu J, Liu J, Ghirlando R, Saltiel AR, Hubbard SR. Structural basis for recruitment of the adaptor protein APS to the activated insulin receptor. Mol Cell. 2003; 12:1379–1389. [PubMed: 14690593]
35. Otwinowski Z, Minor W. Processing of x-ray diffraction data collected in oscillation mode. Methods Enzymol. 1997; 276:307–326.
36. Terwilliger TC, Berendzen J. Automated MAD and MIR structure solution. Acta Crystallogr D. 1999; 55:849–861. [PubMed: 10089316]
37. Emsley P, Cowtan K. Coot: model-building tools for molecular graphics. Acta Crystallogr D. 2004; 60:2126–2132. [PubMed: 15572765]
38. Brünger AT, et al. Crystallography & NMR system: A new software suite for macromolecular structure determination. Acta Crystallogr D. 1998; 54:905–921. [PubMed: 9757107]
39. Murshudov GN, Vagin AA, Dodson EJ. Refinement of macromolecular structures by the maximum-likelihood method. Acta Crystallogr D. 1997; 53:240–255. [PubMed: 15299926]

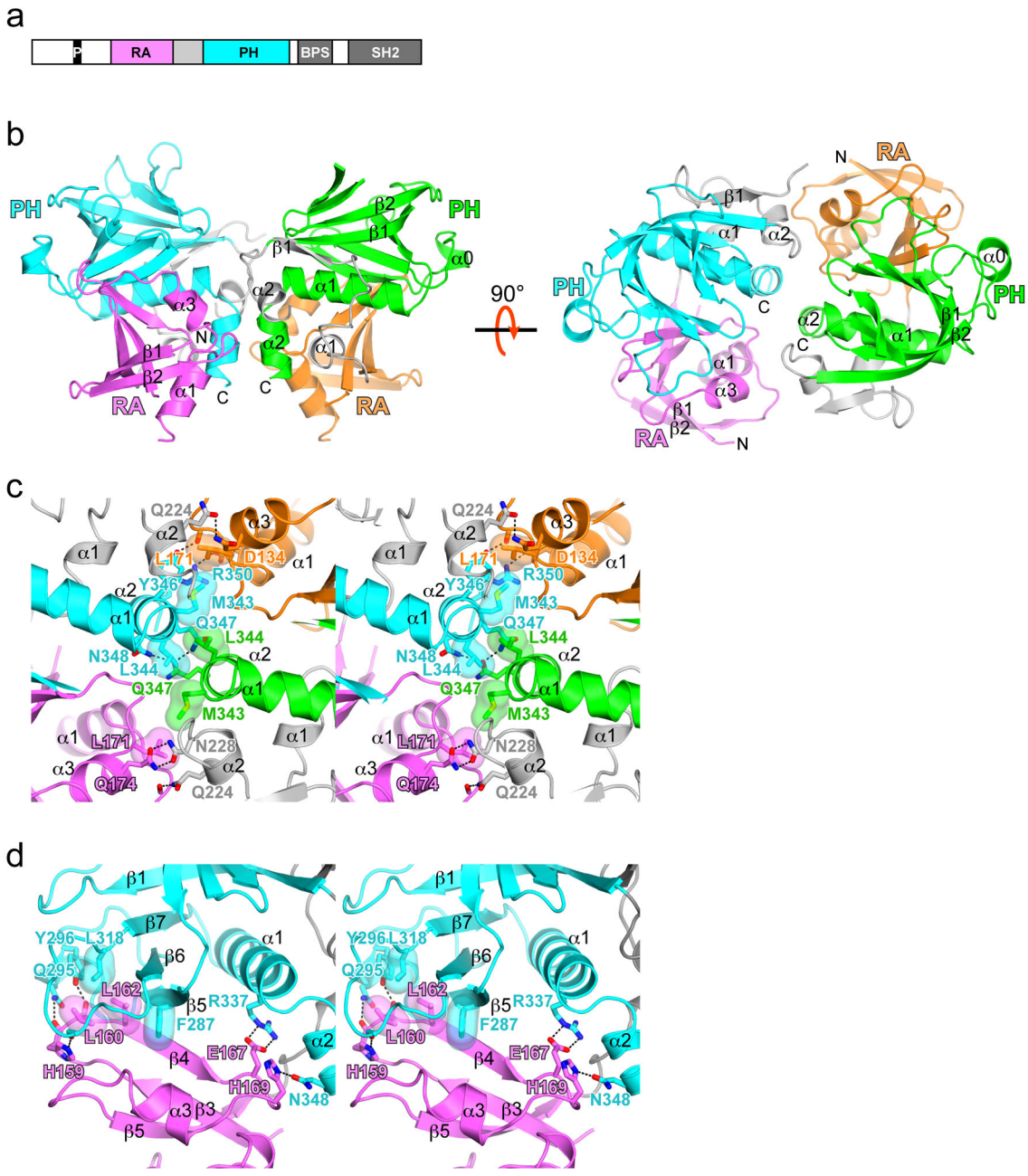

Figure 1.

Crystal structure of human Grb10 RA-PH. (**a**) Domain architecture of Grb7-10-14 drawn to linear scale (human Grb10, isoform c, 536 residues). The abbreviations are: P, proline-rich; RA, Ras-associating; PH, pleckstrin-homology; BPS, between PH and SH2; and SH2, Src-homology-2. (**b**) Ribbon diagram of the crystal structure of Grb10 RA-PH. One copy of RA-PH is colored violet (RA) and cyan (PH), and the second copy is colored orange (RA) and green (PH). For both copies, the RA-PH linker is colored gray. In (b) and (c), the binding sites for small GTPases on the RA domain and phosphoinositides on the PH domain (non-canonically) are indicated by the position of the labels ‘RA’ and ‘PH’. An approximate two-

fold axis (vertical, in the plane of the figure) relates the two molecules in the asymmetric unit. Select secondary-structure elements are labeled, as are the N- and C-termini. In the right panel, the structure has been rotated 90°, as indicated, with the molecular two-fold axis perpendicular to the plane of the figure. (**c**) Stereo view of the dimerization interface. The view is the same as in the right panel of (b). Side chains that mediate the interaction between the two RA-PH molecules are shown in stick representation. Hydrogen bonds/salt bridges are represented by black dashed lines. The side chains of hydrophobic residues are shown with a van der Waals surface. (**d**) Stereo view of the interface between the RA and PH domains. Side chains that mediate the interaction between the two domains are shown in stick representation. Hydrogen bonds/salt bridges are represented by black dashed lines. The side chains of hydrophobic residues are shown with a van der Waals surface. Figures 1, 3c–d, and 6 were rendered with PyMOL (http://pymol.sourceforge.net).

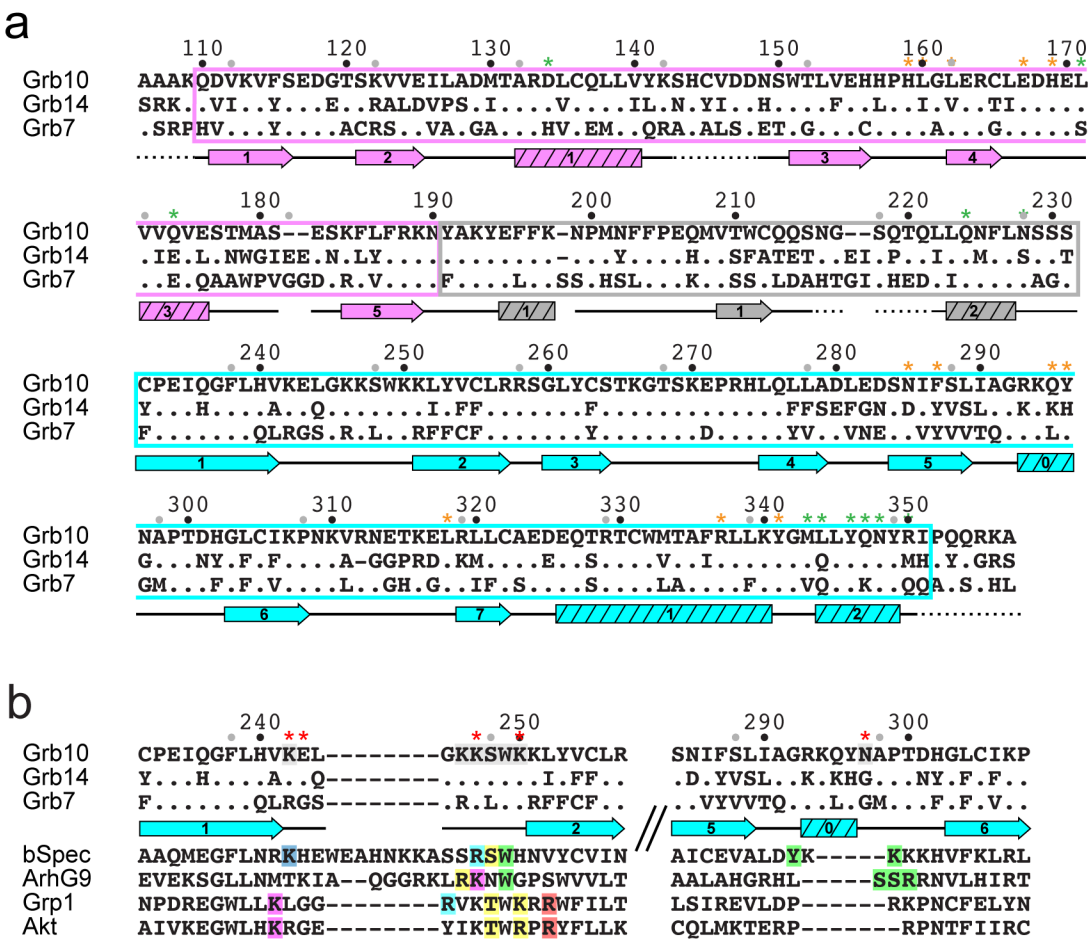

Figure 2.

Structure-based sequence alignments. (**a**) Alignment of the RA and PH domains of human Grb7-10-14. Residues in Grb14 and Grb7 that are identical to those in Grb10 are represented by a period. Secondary-structure elements for Grb10 RA-PH (α helices and β strands) appear below the sequences. A dashed line indicates a disordered region. The RA domain is boxed in violet, the RA-PH linker is boxed in gray and the PH domain is boxed in cyan. Residue numbering is for human Grb10 and Grb14, with the black dots specifying the on-decade numbering for Grb10, and the gray dots specifying the on-decade numbering for Grb14 (same numbering between residues 182-217). Orange and green asterisks indicate residues in the RA-PH interface and the dimerization interface, respectively. (**b**) Alignment of the PH domains of Grb7-10-14 and others. The secondary-structure elements for the Grb10 PH domain are shown below the Grb7 sequence. Two sequence regions are shown: the β1-β2 region and the β5-β6 region. The PH domains of β-spectrin (bSpec)22 and ArhGAP920 bind phosphoinositide headgroups non-canonically, and the PH domains of Grp123,24 and Akt25 bind headgroups canonically. Shaded in gray are Grb10 residues that are potentially involved in non-canonical binding of headgroups. Key to color shading of phosphate-interacting residues in the other PH domains: 1-phosphate (yellow), 3-phosphate (red), 4-phosphate (green), 5-phosphate (cyan), 3- and 4-phosphate (magenta) and 4- and 5-phosphate (blue). Red asterisks mark the residues in Grb10 that were mutated in this study.

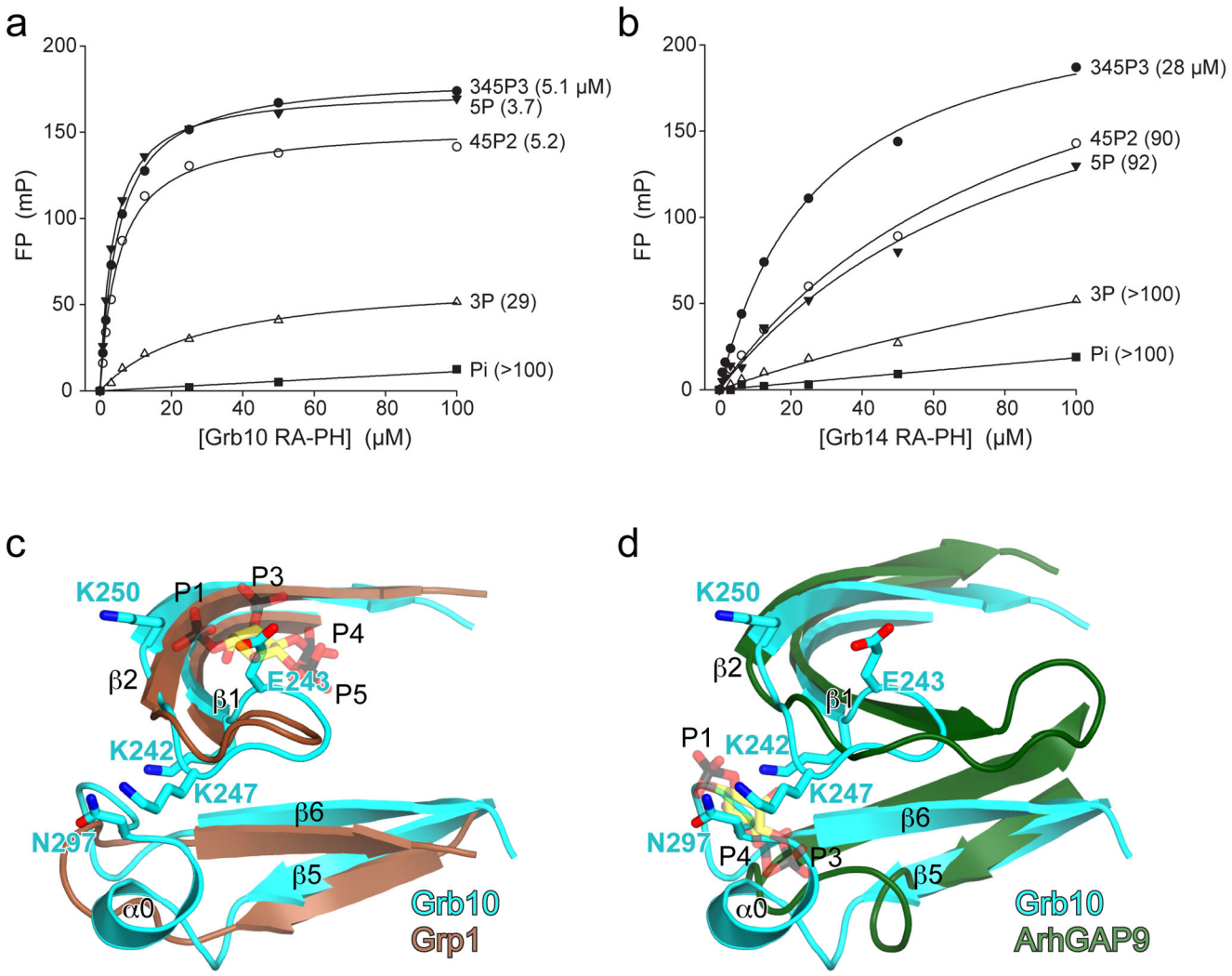

Figure 3.

Binding of phosphoinositides to Grb10 and Grb14 RA-PH. (**a**) Representative fluorescence-polarization measurements (millipolarization (mP) versus protein concentration) of phosphoinositide binding to wild-type Grb10 RA-PH. Fits are based on a saturable, single-site binding model. K_d values (in μM) extracted from the fits are given in parentheses to the right of the headgroup labels and range from 3.7 μM to >100 μM. Complete results are given in Table 2. (**b**) Same as (a), but for Grb14 RA-PH. The K_d values range from 28 μM to >100 μM. (**c**) Comparison of the PH domains of Grb10 and Grp1. Residues in β1 and β2 were superimposed, and for clarity, only β1-β2 and β5-β6 are shown. Grb10 is colored cyan, and Grp1 (PDB code 1FGY)24 is colored brown with the canonically bound Ins(1,3,4,5)P_4 headgroup (semi-transparent) colored yellow (carbon atoms), red (oxygen atoms) and black (phosphorus atoms). The phosphate positions on the inositol ring are labeled. Residues in Grb10 that were mutated in this study are shown in stick representation and labeled. Relative to Grp1, Grb10 contains a 6-residue insertion in the β5-β6 loop. (**d**) Comparison of the PH domains of Grb10 and ArhGAP9. Residues in β1 and β2 were superimposed (identical orientation as in (c)). ArhGAP9 (PDB code 2P0H)20 is colored green with the non-

canonically bound Ins(1,3,4)P_3 headgroup (semi-transparent) colored as in (c). Relative to Grb10, ArhGAP9 contains a 6-residue insertion in the β1-β2 loop and a 5-residue deletion in the β5-β6 loop.

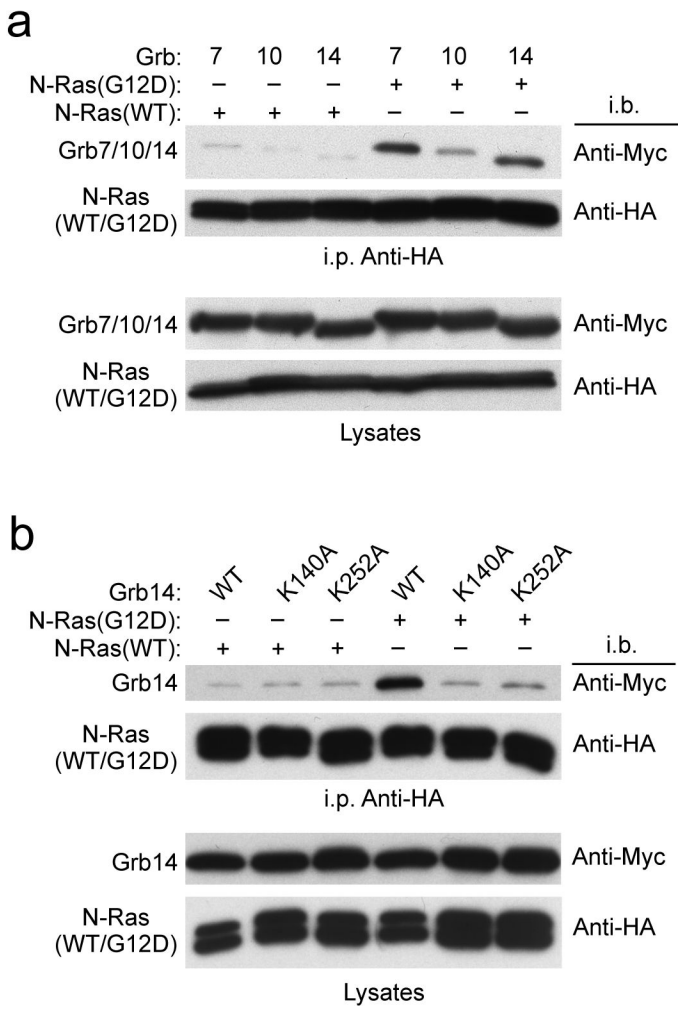

Figure 4.

Interaction between Grb7-10-14 and Ras. (**a**) Co-immunoprecipitation (i.p.) of Myc-tagged Grb7, -10, or -14 with HA-tagged wild-type N-Ras or N-Ras G12D (constitutively activated) from HEK 293T cells. Antibodies used for immunoblotting (i.b.) are indicated on the right sides of the blots, and protein identifications are supplied on the left sides. The bottom blot of the anti-HA immunoprecipitations and the two blots of the lysates are controls for protein levels. (**b**) Same co-immunoprecipitation experiment as in (a), but with Myc-tagged Grb14, either wild-type or K140A (RA) or K252A (PH), along with wild-type N-Ras or N-Ras G12D.

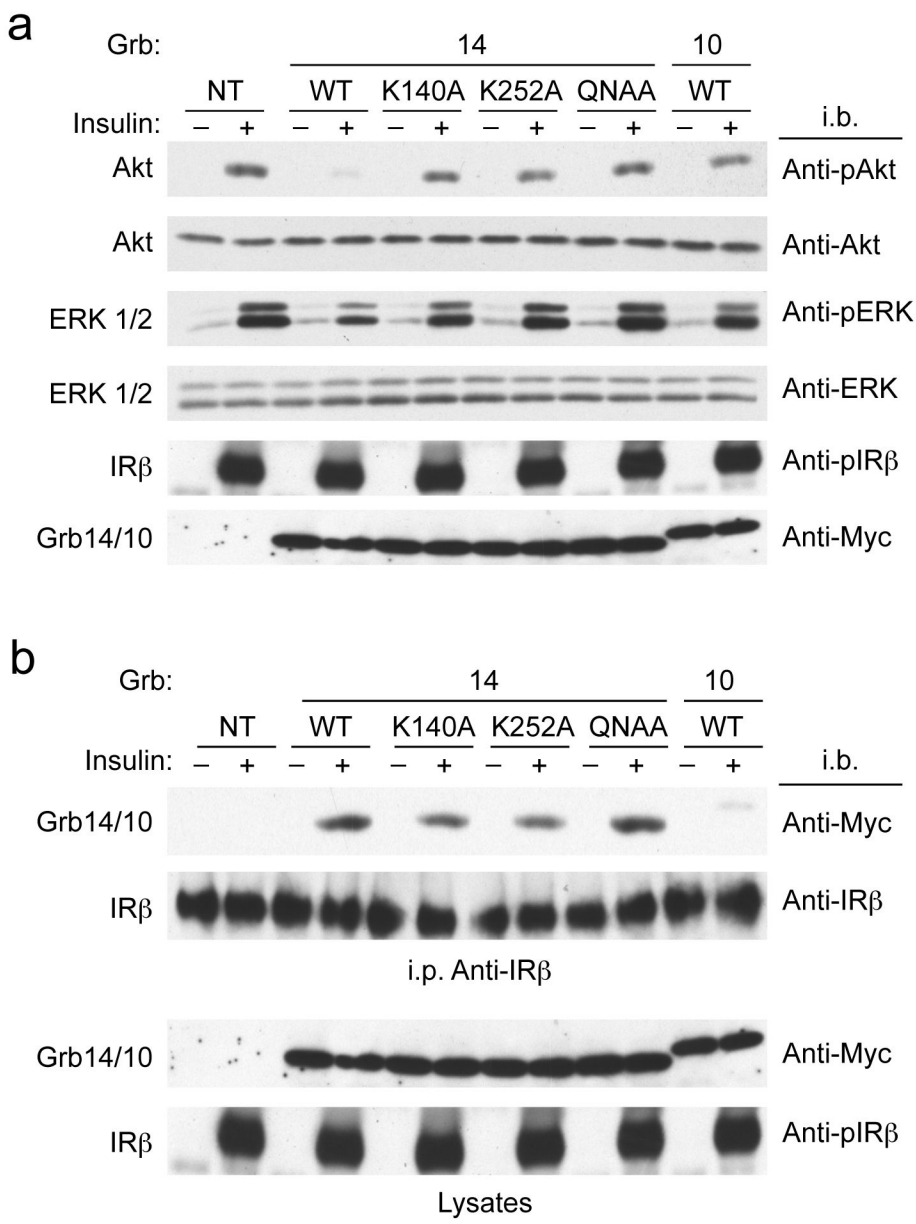

Figure 5.

Inhibition of insulin signaling by Grb14/10. (**a**) Immunoblotting (i.b.) of lysates from insulin stimulated (or not) CHO-IR cells transfected with Myc-tagged Grb14, wild-type or the specified point mutant (K140A (RA), K252A (PH), QNAA (Q348A/N349A, dimerization interface)) or Myc-tagged Grb10 (wild-type). The antibodies used are shown on the right sides of the blots, and protein identifications are given on the left sides. (NT: non-transfected) (**b**) The lysates from (a) were subjected to immunoprecipitation (i.p.) using the anti-insulin receptor βsubunit (anti-IRβ) antibody, and immunoblotting was performed with the antibodies indicated on the right sides of the blots.

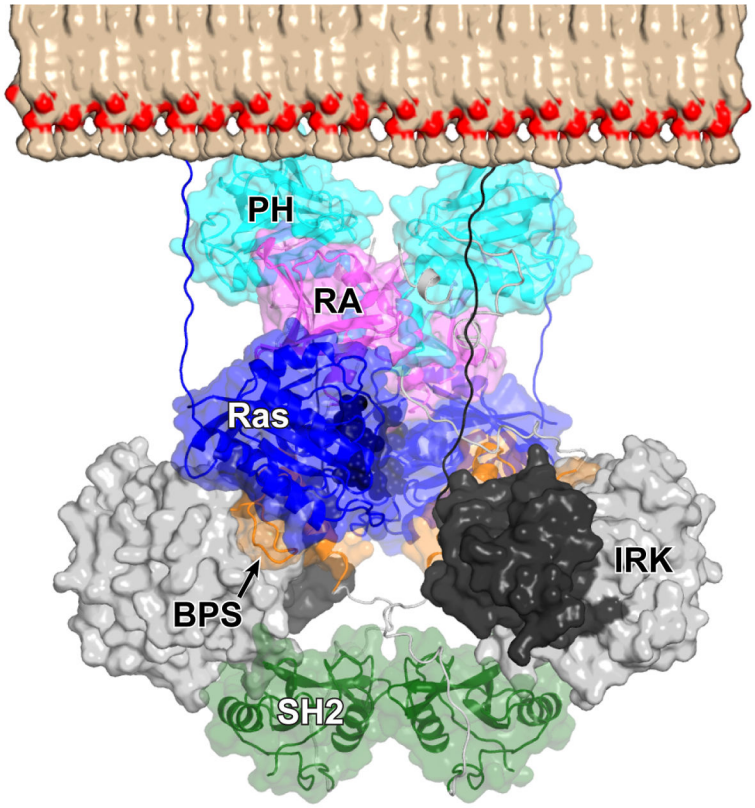

Figure 6.

Model of the interaction between Grb14, Ras and the insulin receptor. The two insulin receptor kinase (IRK) domains are shown in surface representation (opaque) colored dark (N lobe) and light (C lobe) gray. The juxtamembrane regions linking the transmembrane helices to the kinase domains are colored black. Grb14 is shown in ribbon representation with a semi-transparent surface. The RA domain is colored violet, the PH domain cyan, the BPS region orange and the SH2 domain green. The interdomain linker regions are colored gray. Two Ras molecules (colored blue) are shown in ribbon representation with semi-transparent surfaces. The bound nucleotide (GMPPNP) is shown in sphere representation and colored black. Starting from the structure of IRK-Grb14(BPS) (PDB code 2AUH)10 (two copies), the dimeric SH2 domain of Grb14 (PDB code 2AUG)10 was docked onto the two IRK molecules based on the structure of IRK-APS(SH2) (PDB code 1RQQ)34. The molecular two-fold axis of the SH2 dimer is perpendicular to the plane of the membrane (half of a lipid bilayer is depicted to scale). Ras was docked onto Grb10 RA-PH using the structure of the Ras-RalGDS(RA) complex (PDB code 1LFD)27. The two-fold axis of RA-PH is perpendicular to the membrane (oriented as in Fig. 1b, left). The juxtamembrane region of the insulin receptor, the interdomain linkers of Grb14 and the C-terminal tail of N-Ras were modeled using stereochemically realistic polypeptide segments. For the C-terminal segment of N-Ras, residues Lys167 through Cys181 (the site of palmitoylation, five residues N-terminal to the CAAX box) are modeled in an extended conformation. Because of the degrees of freedom inherent in assembling the model, it is difficult to speculate whether Ras might interact directly with IRK or the Grb14 BPS region.

Table 1

Data collection and refinement statistics

	Native	SeMet
Data collection		
Space group	*C2*	*C2*
Cell dimensions		
a, *b*, *c* (Å)	126.9, 48.9, 92.2	125.9, 48.8, 92.1
α, *β*, *γ* (°)	90, 114.1, 90	90, 114.3, 90
Wavelength	0.9787	0.9789
Resolution (Å)	50.0-2.6	50.0-2.6
R_{sym} or R_{merge}	6.2 (32.3)*	4.6 (32.9)*
$I / \sigma I$	13.8	13.0
Completeness (%)	99.6 (99.4)*	99.2 (94.1)*
Redundancy	3.9	3.8
Refinement		
Resolution (Å)	2.6	
No. reflections	15,264	
R_{work}/R_{free}	23.0/27.7	
No. atoms		
Protein	3,525	
Solvent	17	
B-factors		
Protein	48.9	
Solvent	47.5	
R.m.s deviations		
Bond lengths (Å)	0.007	
Bond angles (°)	1.0	

*Values in parentheses are for highest-resolution shell. One crystal was used for each data set. TLS (translation/libration/screw) parameters for each protomer were included in the refinement.

Table 2

Phosphoinositide binding constants

	$345P_3$	$34P_2$	$35P_2$	$45P_2$	3P	4P	5P	Pi
Grb10								
WT	5.1	5.5	10	5.2	29	20	3.7	>100
K242A	10	11	17	11	n.d.	n.d.	5.5	>100
E243G/L244S	4.5	11	36	12	37	34	13	>100
K247A	26	60	80	34	>100	>100	36	>100
K250A	28	27	n.d.	n.d.	25	n.d.	21	n.d.
N297G	26	34	78	32	n.d.	n.d.	16	>100
Grb14								
WT	28	99	>100	90	>100	>100	92	>100
E245G/Q246S	8.3	19	n.d.	17	n.d.	n.d.	18	n.d.
K252A	>100	>100	>100	>100	>100	>100	>100	>100
G299N	34	>100	>100	>100	>100	>100	>100	>100
Grp1	0.016	n.d.	n.d.	0.72	n.d.	n.d.	3.6	n.d.

K_d values in μM. n.d. = not determined. Grb10 and Grb14 RA-PH proteins were used in the binding experiments. The PH domain of Grp1 was used as a control in the fluorescence-polarization assay.